NASA Technical Memorandum 82599

Oxidation-Induced Contraction and Strengthening of Boron Fibers

James A. DiCarlo and Timothy C. Wagner
Lewis Research Center
Cleveland, Ohio

Prepared for the
Fifth Annual Conference on Composites and Advanced Materials
sponsored by the American Ceramic Society
Merritt Island, Florida, January 18-22, 1981

NASA

OXIDATION-INDUCED CONTRACTION AND STRENGTHENING OF BORON FIBERS*

by James A. DiCarlo and Timothy C. Wagner

National Aeronautics and Space Administration

Lewis Research Center

Cleveland, Ohio 44135

ABSTRACT

An investigation was conducted to measure and understand the physical and mechanical effects that occur in boron fibers during and after thermal treatment in a controlled oxygen-argon gaseous mixture. Of principal concern was the optimization of this treatment as a secondary processing method for significantly improving fiber tensile strength. Strengthening was accomplished by an oxidation-induced axial contraction of the fiber and a resulting axial compression of strength-limiting flaws within the fiber's tungsten boride core. Although contraction strains above 4 percent were easily obtained for 203 μm (8 mil) diameter fibers, strengthening was not achieved for contractions above 0.3 percent due to the formation of new flaws in the boron sheath. Nevertheless, after a 0.3 percent oxidation-induced contraction near 900° C and a slight surface etch near 100° C, the average tensile strength of the 203 μm fibers increased from 3.4 GN/m^2 (500 ksi) to 5.5 GN/m^2 (800 ksi) and the strength coefficient of variability decreased from ~15 percent to less than 5 percent. Various physical observations were used to develop mechanistic models for oxidation, contraction, and new flaw formation. Processing guidelines are discussed for pos-

---

*Presented at the Fifth Annual Conference on Composites and Advanced Materials sponsored by the American Ceramic Society, Merritt Island, Florida, January 18-22, 1981.

and permanent axial contraction of the boron sheath that surrounds the core. Because of the small size of the core and its good bond with the sheath, the axial contraction compressed the elastic core thereby raising the stress and strain levels required to initiate core-induced fiber fracture. Under this condition, if E is the fiber modulus and ε_z is the treatment-induced axial fiber contraction strain, fiber tensile strengths were increased by the product $E\varepsilon_z$. DiCarlo concluded that probably the most simple and cost-effective secondary treatment was that in which the commercial fibers were heated in impure argon gas at temperatures near 900° C. It appeared that by reacting with an unidentified impurity in the argon, boron atoms were removed from within the sheath causing the fiber to contract axially and core flaws to be compressed (6). Using this heat treatment method and a subsequent surface etch treatment near 100° C, DiCarlo observed the room temperature strength of 203 μm (8 mil) diameter fibers to increase proportionally with ε_z up to 0.3 percent after which point the fiber strength began to drop off significantly due to the formation of new fracture-controlling flaws within the boron sheath. However, even with this limitation, the average tensile strength of the 203 μm fibers was improved from 3.4 GN/m^2 (500 ksi) to 5.5 GN/m^2 (800 ksi).

In terms of impact resistance, the practical advantage of the combined use of the impure argon and etch treatments becomes evident when one realizes that by raising fiber tensile strengths to 5.5 GN/m^2 (800 ksi), the tensile work of fracture is improved to more than twice that of the as-produced fiber. The fact that the CVD sheath has shown strength potential over 6.9 GN/m^2 (1000 ksi) indicates the possibility for still further improvement if the formation mechanisms for the new sheath flaws could be understood and possibly avoided. Thus the objectives of this study were to

measure and understand the physical and mechanical effects of heat treating boron fibers in impure argon gas so that this treatment method might be optimized as a secondary processing technique for boron fiber strength improvement. Although no definite identification of the impurity gas responsible for contraction was obtained in previous work, the recent results from the boron fiber contraction study of Wawner, et al. (7) pointed to oxygen as the most likely impurity. For this reason the approach taken here was to broaden the impure argon studies by also measuring the effects of heat treating fibers in oxygen-argon gaseous mixtures containing much higher and better controlled oxygen contents. It will be shown that although the high oxygen approach did not achieve any additional strengthening for temperatures below 900° C, it did aid in clarifying the physical processes that occurred during treatment and by so doing also indicated possible processing conditions for further strength improvement.

EXPERIMENTAL PROCEDURE

The specimens used in this study were 203 μm (8 mil) diameter fibers commercially supplied by Avco Specialty Materials Division. These fibers were produced in a single stage CVD reactor by the hydrogen reduction of boron trichloride on a 13 μm (0.5 mil) diameter tungsten wire substrate. Deposition temperatures were maintained near 1300° C by dc resistance heating augmented by very high frequency heating (8). During deposition the substrate became completely borided to form a 17 μm diameter tungsten boride core. From previous studies (4,5) it was determined that the 203 μm boron fiber produced in the above manner is excellent material for achieving strengthening by core compression because in the as-received condition the probability for observing core-initiated fracture after a slight surface etch is essentially 100 percent.

The apparatus employed for the oxidation-contraction studies is shown schematically in Fig. 1. It is a glass column, similar to a commercial CVD reactor, in which a static fiber is resistance heated within a controlled gaseous environment. Water-cooled stainless steel caps at each end of a 2.5 cm diameter pyrex tube contained inlet and outlet gas ports and mercury seals for electrical contact to the boron sheath. Prior to insertion in the reactor, each fiber was wiped with methanol to remove any existing boron oxide layers. Within the reactor the fiber was clamped above the top end cap and subjected to a minimal clamp weight of 9 grams below the lower cap. Fiber length changes due to thermal expansion and oxidation-induced contraction were measured at the lower fiber end with a traveling microscope. By varying the pyrex tube length between 16 and 64 cm, it was determined that the axial strain measurements were independent of the length of heated fiber. Errors in the strain data were estimated to be less than 0.002 percent.

The principal variables in this study were time, temperature, and the partial pressure of oxygen within an argon carrier gas. Purity analyses for the two gases are listed in Table I. Prior to each heat treatment run, the volume fractions of oxygen and argon were set by adjusting the input flow rates of the two gases into a mixing chamber in line with the reaction chamber. The gas mixture entered the reactor at 1 atmosphere at constant flow rates from 50 to 500 cc/min. After adjustment and stabilization of gas pressure and flow, the change in fiber length was measured as the applied dc current was quickly (~10 sec) increased from zero to a preset value which was held constant throughout the entire run. At the conclusion of the run, current was quickly (~10 sec) dropped to zero. During the short warmup and cooldown periods, fiber length changed due to thermal expansion effects;

whereas at high temperature, fiber length decreased primarily due to oxidation-induced contraction effects.

The fiber temperature during heat treatment was conveniently determined by comparing the average thermal expansion strain observed during warmup and cooldown with the expansion versus temperature plot of Fig. 2. Data points for this calibration plot were determined from average strain data and optical pyrometer measurements taken during the course of a typical contraction run. The pyrometer data were corrected for a fiber surface emissivity of 0.63 ± 0.07 which is the best fit value calculated from experimental power losses by gas conduction and fiber radiation. Due to the rapid oxidation of the boron fiber surface, this emissivity value is most likely that of boron oxide. The curve of Fig. 2, which allows extrapolation to lower temperatures, is the best fit theoretical expansion curve for amorphous boron using Gruneisen's equation (9).

It was observed that the thermal expansion strain during cooldown was often slightly smaller than the expansion strain during warmup (a difference of less than 0.01 percent strain). Or, put in another way, the total contraction measured at the processing temperature was slightly greater (by less than 0.01 percent strain) than the contraction measured at room temperature. This difference was due to a slight cooling of the fiber during the constant current heat treatment. Controlled studies indicated that cooling arose from two mechanisms. First, for a clean as-received fiber, the formation of boron oxide appears to increase fiber emissivity, resulting in a slightly greater radiation loss and a consequent fiber cooling. Second, monitoring of reactor voltage indicated a small but continuous voltage decrease during oxidation. The decrease was directly proportional to heated fiber length, indicating that its source was a decreasing fiber resistance. Thus power input to the fiber diminished

slightly during oxidation, resulting in another source of specimen cooling. It is estimated, however, that under the constant current heating technique the two cooling effects produced less than a 10° C drop in fiber surface temperature during an entire run. Therefore the error in the temperature determination was less than ±5° C.

After heat treatment and prior to measurement of their physical and mechanical properties, the contracted fibers were again wiped with methanol to remove boron oxide surface layers. Measurements were then made of fiber mass, diameter, and tensile strength. The techniques and accuracies of these measurements are discussed elsewhere (10). Prior to the strength tests, the contracted fibers were slightly etched in fuming nitric acid near 100° C (4) to remove the original as-received surface flaws and any additional surface flaws introduced during the oxidation process. The fibers were then pulled to failure in tension at room temperature. The 2.5 cm gauge length section was coated with vacuum grease in order to damp out fracture-induced stress waves which can intensify by reflection off the grips and thus create multiple fracture sites. This test procedure thus produced only the two original fracture surfaces which were retained for subsequent study by optical and scanning electron microscopy (SEM).

RESULTS AND DISCUSSION

One of the prime objectives of this study was to optimize the oxygen-argon thermal treatment as a secondary processing method for improving the tensile strength of commercial boron fibers. Because optimization depends strongly on an understanding of treatment-related microstructural processes, the results that follow are discussed with the goal of obtaining a physical insight into these mechanisms. Thus the first section presents the empirical results for the effects of time, temperature, and oxygen content on the

magnitude of axial contraction. These results are then combined in the second section with physical property data on contracted fibers in order to develop plausible models for the mechanisms involved in oxidation and contraction. Finally, in the last section the tensile strength and flaw formation results are presented and examined in light of the mechanistic understanding developed in the first two sections.

Contraction Kinetics

Typical contraction results for heat treatment in the impure argon with no added oxygen are shown in Fig. 3. Close examination of these results revealed that after about 5 minutes of heating, the axial contraction strain ϵ_z followed a parabolic dependence on time t. That is, the curves for ϵ_z could be fit very well to the empirical equation

$$\epsilon_z(\text{percent}) = \frac{\alpha(t)^{1/2}}{d} - \epsilon_z^0 \qquad (t > 5 \text{ min}) \qquad (1)$$

where ϵ_z^0 is a small constant, d is the fiber diameter, and α is a parameter which, as will be shown, is temperature and oxygen dependent but is independent of fiber diameter. This parabolic behavior with time can be seen in Fig. 4 where the Fig. 3 data have been replotted as a function of $t^{1/2}$. When the oxygen volume fraction in the argon was increased to 1, 10, and 50 percent, all contraction curves for temperatures between 650° and 900° C and contraction strains up to 2 percent were also observed to be parabolic in time according to Eq. (1). A typical example is given in Fig. 5 which shows contraction strain data for 50 percent oxygen content at 794° C. Actual data points are not shown because they were measured every 30 sec with an error of less than 0.002 percent.

The source of the non-parabolic behavior at short times in not yet understood. It may be an indication that 2 to 5 minutes are required to

reach equilibrium conditions on the fiber surface or that the as-produced fibers display a small but real expansion during the initial stages of heat treatment. However, whatever the source, one can in many cases neglect this effect and assume a parabolic time dependence throughout an entire run. That is, the empirical constant ϵ_z^o in Eq. (1) can be neglected since it was always observed to be small, falling in the range 0.07±0.05 percent.

Increasing temperature and/or oxygen content produced an increase in contraction rate. This is evidenced in the Fig. 6 data for the log of the α parameter from Eq. (1) as a function of reciprocal absolute temperature for all oxygen volume fractions used, including the impure argon case. As will be discussed, there exists ample evidence for assuming that the 0.01 percent oxygen content in the impure argon was responsible for contraction. Also included in Fig. 6 are calculated α parameter data (dashed line) taken from the contraction study of Wawner, et al. (7) in which 102 μm (4 mil) diameter boron on tungsten fibers were heated in dry air. Their limited time-dependent data at 900° C could be fit well to parabolic behavior, although the authors assumed an exponential saturation type of behavior. Using their temperature-dependent results for 5 minute runs, we have assumed the validity of Eq. (1) and calculated α for 21 percent oxygen content.

The linearity of log α with reciprocal absolute temperature is indicative of the fact that contraction is controlled by a thermally-activated process. That is, the α parameter obeys the Arrhenius relation $\exp(-Q/2kT)$ where Q is the controlling thermal activation energy, k is the Boltzmann constant, and T is absolute temperature. For processing temperatures from 650° to 900° C, the energy Q was found to be essentially independent of temperature and oxygen content with a best fit value of

1.46±0.15 eV. The fact that the impure argon results displayed the same parabolic time dependence controlled by the same energy as, for example, the 50 percent oxygen results is considered as strong evidence in support of the controlling role of oxygen in the impure argon data.

Regarding the oxygen dependence for α, it was found that for an oxygen volume fraction v_{O_2} of 1 percent or greater, α was directly proportional to the one-third power of v_{O_2}. The excellent fit for this dependence can be seen in Fig. 7 for a temperature of 875° C. The reason that the α for 0.01 percent oxygen did not follow the one-third power dependence is not understood as yet. Combining the temperature and oxygen dependence for α, one can write that for temperatures from 650° to 900° C and $v_{O_2} \geq 1$ percent,

$$\alpha = \alpha_0 (v_{O_2})^n \exp\left(\frac{-Q}{2kT}\right) \tag{2}$$

which when best fitted to the Fig. 6 data yields

$$\alpha\left(\frac{\mu m}{min^{1/2}}\right) = 28\ 000 (v_{O_2})^{1/3} \exp\left(\frac{-8480}{T}\right).$$

In summary, one can now predict by use of Eqs. (1) and (3) the amount of contraction strain that can be achieved in boron fibers by heat-treating in a partial pressure of oxygen. It is believed that this contraction is controlled by the formation of a thin boron oxide layer on the fiber surface. The physical facts and reasoning in support of this model are discussed in the following section.

Contraction Mechanisms

In previous studies using only impure argon (5,6) a contraction model was developed in which, by reacting with an impurity gas in the argon, boron atoms were removed from within the sheath, leaving behind microvoids with a

smaller average volume than the removed atoms. Three primary questions left unanswered were the identity of the impurity gas, the nature of the physical mechanism controlling contraction kinetics, and the manner in which boron atoms were removed from the sheath. The first question was answered in the preceeding section where the kinetic results strongly support oxygen as the responsible impurity. In this section, answers to the second and third questions will be developed in the light of certain physical observations made during and after thermal treatment under various oxygen conditions.

Regarding the nature of the rate-limiting mechanism controlling contraction, one can envision in terms of the above contraction model at least six processes that could be responsible: (1) diffusion of oxygen through the argon gas; (2) disassociation and/or adsorption of oxygen on the fiber surface; (3) diffusion of boron or oxygen through a boron oxide layer; (4) reaction of the oxygen with boron; (5) formation of a boron atom vacancy or microvoid within the CVD sheath; and (6) migration of the boron atom in the sheath. However, the observations of this study which show that the controlling process is thermally activated and gives rise to a parabolic time dependence strongly suggest that Process 3 was controlling. That is, physical phenomena associated with the oxidation of metals often display a parabolic time dependence because one of the reacting atom species must diffuse through an oxide layer which is continuously growing with time (11). If h is the oxide thickness, the rate of oxide growth dh/dt is inversely proportional to h which means that h follows a $t^{1/2}$ dependence. This parabolic thickness growth implies in turn that the number of boron atoms removed from the sheath and the resulting axial contraction should also follow a parabolic time dependence.

Convincing experimental evidence for the controlling nature of the boron oxide layer was obtained by removing a contracted fiber from the reactor, wiping the surface with methanol to remove the oxide layer, and rerunning the same fiber under identical temperature and oxygen conditions. Instead of continuing on the previous contraction curve as would be observed if the specimen were cooled to room temperature and then reheated without cleaning, the fiber exactly repeated the original time dependence curve as if it were a clean as-received specimen. Thus after wiping, the fiber displayed no evidence of previous contraction, indicating contraction kinetics were not controlled by a mechanism within the fiber but by a mechanism associated with the boron oxide layer. Identifying this mechanism as atomic diffusion through the oxide, one can then relate the contraction energy Q to the oxide diffusion energy and the contraction oxygen dependence to the formation of those atomic defects required for diffusion (11).

At contractions above 2 percent the boron oxide layer was actually visible on the fiber surface during heat treatment. This was caused by the fact that due to surface tension forces and a liquid nature at the processing temperatures (12), the oxide layer began to form beads, giving the fiber an obvious beaded appearance. This in turn produced a beaded fiber surface (observed after the run) due to more rapid removal of boron atoms near the thinner parts of the boron-oxide beads. At the bead formation point the contraction curve changed from parabolic to approximately linear with time. Under these conditions, contraction strains greater than 4 percent were produced with no apparent evidence of saturation effects. The beading phenomenon offers additional support for the controlling nature of oxide growth on contraction kinetics.

To develop the quantitative aspects of boron oxide growth and boron atom removal, measurements were made of fiber mass per unit length before and after heat treatment under a variety of processing conditions. Prior to each measurement the fibers were wiped with methanol to remove the boron oxide. This was necessary to eliminate variability in the mass measurements caused by the hydroscopic nature of the oxide. The results for $\Delta M/S$, the mass of boron atoms removed per unit surface area of the original 203 μm diameter fibers, are shown in Fig. 8 as a function of axial contraction strain ϵ_z. The change in mass ΔM was normalized by the fiber surface area S to reflect the fact that the mass removal was caused by an oxidation process on exposed fiber surfaces. Thus the property $\Delta M/S$ should only be time, temperature, and oxygen dependent and should be independent of fiber diameter.

The Fig. 8 data indicate that $\Delta M/S$ increased linearly with ϵ_z; i.e., for a 203 μm fiber,

$$\frac{\Delta M}{S}\left(\frac{mg}{cm^2}\right) = (0.37 \pm 0.03)\epsilon_z. \tag{4}$$

This result suggests that the amount of mass removed was dependent only on the magnitude of ϵ_z and not on the time, temperature, or oxygen condition utilized to produce ϵ_z. It also supports the model that the source of fiber contraction up to at least 4.4 percent was simply the direct removal of boron atoms. It follows then that the kinetics which govern contraction also govern atom removal. Thus, from Eqs. (1), (3), and (4), and the assumption $\epsilon_z^0 = 0$,

$$\frac{\Delta M}{S}\left(\frac{mg}{cm^2}\right) = 0.0018\ \epsilon_z d(\mu m) = 51\ t^{1/2}\ (v_{O_2})^{1/3} \exp\left[\frac{-8480}{T}\right] \tag{5}$$

This general experimental result for fiber oxidation in time t (min) applies for oxygen volume fractions $v_{O_2} \geq 1$ percent and fiber temperatures from 650° to 900° C.

One can estimate the thickness h_o of an oxide layer during contraction by assuming all removed boron atoms enter into a stoichiometric boron oxide layer. If $h_o \ll d$, it follows from mass considerations that

$$h_o = \left(\frac{\Delta M}{S}\right)\left[\frac{\eta_O}{\eta_B v_B \rho_O}\right] \tag{6}$$

where η_O and ρ_O are the atomic weight and density of boron oxide and η_B and v_B are the atomic weight of boron and its stoichiometric ratio ($v_B = 2$) in boron oxide (B_2O_3). Thus h_o is independent of fiber diameter and grows parabolically with time. To estimate its value for a fiber of diameter d after contraction ϵ_z, one can use Eqs. (5) and (6) and $\rho_O \cong 1.6$ gm/cc (12) to calculate that $h_o(\mu m) \cong 0.04\ \epsilon_z d(\mu m)$. Thus $h \cong 8$ μm after 1 percent contraction of a 203 μm fiber.

The mass loss result can also be useful in understanding some of the microstructural processes that occurred within the sheath as boron atoms were removed from the fiber. This understanding will be used in the next section to interpret mechanisms for new flaw formation. In general, in order to explain axial contraction during oxidation, one must assume that not all vacancies or microvoids resulting from atom removal were created on the external fiber surface but that a certain fraction were formed within the sheath. Direct physical evidence in support of this can be found in the SEM photos of Fig. 9. These show that after about 0.7 percent axial contraction, small voids appeared at the core-sheath interface and then grew larger with higher contraction. Similar interface behavior was also observed by Wawner, et al. (7). Thus during oxidation at the surface, boron

atoms were removed from the deepest regions of the sheath, implying the existence of fast diffusion paths from core to surface. To understand these sheath phenomena, it is of interest to develop a mathematical model for axial contraction and then to quantify this model with mass loss and diameter data.

If ΔV_i is the volume decrease caused by the creation of internal microvoids, the resulting axial contraction strain is given by

$$\epsilon_z = \gamma_z \left(\frac{\Delta V_i}{V}\right)$$

where V is the fiber volume and γ_z is a parameter which measures the fraction of internal volume change that takes place in the axial direction. Because ΔV_i results from the removal of atoms with an atomic volume Ω_B and the creation of microvoids with an average volume Ω_B', it follows that

$$\Delta V_i = \beta \Delta N (\Omega_B - \Omega_B')$$

where ΔN is the total number of atoms removed from the fiber and β is that fraction removed from within the sheath. Thus, since $V = N\Omega_B$, the theoretical formula for ϵ_z in terms of total atoms removed is

$$\epsilon_z = \beta \gamma_z (1 - R) \left(\frac{\Delta N}{N}\right)$$

where $R \equiv \Omega_B'/\Omega_B$, the ratio of internal microvoid volume to atom volume. Because

$$\frac{\Delta N}{N} = \frac{\Delta M}{M} = \left(\frac{\Delta M}{S}\right)\left(\frac{4}{\rho_B}\right)\frac{1}{d} \qquad (7)$$

it follows, as was assumed in Eq. (1), that ϵ_z should be inversely proportional to fiber diameter α. Using a sheath density ρ_B of 2.35 gm/cc (10) and the mass loss result of Eq. (4), one finds that the microstructural parameters are related by

$$\beta\gamma_z(1 - R) = 0.32 \pm 0.03 \tag{8}$$

To further quantify these parameters, measurements were made of fiber diameter before and after oxidation under various conditions. The results are plotted in Fig. 10 in terms of radial contraction strain ϵ_r versus axial contraction strain. These data indicate a strain equality which is independent of processing conditions, implying that a uniform contractive dilatation occurred as atoms were removed from the fiber. In theory, this total volume decrease was caused by the internal volume decrease ΔV_i plus an external volume decrease $(1 - \beta)\Delta N\Omega_B$ due to boron atom removal from the original fiber surface. It follows then that

$$\frac{\Delta V}{V} = 2\epsilon_r + \epsilon_z = 3\epsilon_z = [\beta(1 - R) + (1 - \beta)]\left(\frac{\Delta N}{N}\right)$$

so that from Eqs. (4), (7), and (8),

$$\beta\gamma_z = 0.32 \pm 0.03 + \gamma_z(0.01 \pm 0.09)$$

$$\beta R = 0.01 \pm 0.09.$$

The result for $\beta\gamma_z$ implies that if atomic relaxation around internal microvoids was equal in all directions, $\gamma_z = 1/3$ and $\beta \approx 1$. Since it would be difficult to envision a γ_z greater than 1/2 (2-dimensional relaxation), it follows then that a majority of oxidation-induced microvoids ($\beta > 1/2$) were created within the sheath and not on the fiber surface. This conclusion is supported by the SEM photos of Fig. 11 which show that the fiber surface (after removal of the oxide) changed little during contrac-

tion. The only apparent topographical effects were the growth in size and spatial density of small boron surface crystals (5,6).

The result for βR is also interesting in that for large β, R is near zero, implying almost complete relaxation of atoms surrounding the internal microvoids. This suggests that these microvoids were created on inner surfaces within the sheath rather than being formed randomly in continuous sheath material were incomplete relaxation might be expected (R value nearer to unity). The fact that at least one type of inner surface does indeed exist within the CVD sheath can be seen in the photos of Fig. 11. These show clearly the boundaries between the so-called kernels which nucleate on the tungsten substrate surface and grow during deposition as individual entities to create the corn-cob appearance on the fiber surface (12). The fact that the kernel boundaries extend from the tungsten-boride core to the fiber surface suggests that perhaps these boundaries were not only the inner sheath surfaces at which the low-volume microvoids were formed but were also the fast diffusion paths which allowed atom removal at the core-sheath interface. Thus the physical observations and data support a model in which the primary boron atom sources for the oxide layer were loosely-bound surface atoms which migrated from inner kernel boundary surfaces to the external kernel surface. During the initial stages of contraction, boundary atoms nearest the external surface replaced those atoms removed by oxidation. This set up a concentration gradient which allowed boundary atoms deeper in the sheath to migrate toward the exterior surface. Eventually near the 0.7 percent contraction level (for 203 μm fibers), the loss of boundary atoms at the core-sheath interface reached a point that the visible voids of Fig. 9 were formed.

Finally, as previously discussed, the contraction rate up to 900° C is limited by atom diffusion through the oxide layer. Diffusion of boron within the sheath thus appears to be more rapid than atom motion in the oxide. Eventually, however, at higher temperatures and/or higher oxygen pressures, atom removal at the external surface may become so rapid that the contraction rate becomes limited by sheath diffusion. The nonlinearity of the high temperature α data of Wawner, et al. (7) shown in Fig. 6 may indeed indicate such a phenomenon.

Fiber Strength

In the as-received condition prior to contraction, the commercial fibers used in this study contained only two types of flaws capable of initiating fiber fracture at stress levels below 6.9 GN/m^2 (1000 ksi). One type was located on the fiber surface and the other within the fiber core. Removal of the first type by a slight surface etch produced dramatic effects on fiber strength properties. For example, the minimum flexure strength increased from 3.4 GN/m^2 (500 ksi) to well over 6.9 GN/m^2 (1000 ksi); the average tensile strength for a 2.5 cm test section increased from near 3.4 GN/m^2 (500 ksi) to 4.2 GN/m^2 (630 ksi); and the coefficient-of-variability (COV) for the tensile strength decreased from ~15 percent to less than 5 percent. Examination of the tensile fracture surfaces indicated that all cases of etched-fiber fracture were initiated by core flaws. Thus the very low COV after etching is a unique characteristic of core-initiated fracture.

To determine the effects of oxidation processing on tensile strength, contracted fibers were removed from the gas reactor, cleaned with methanol, and broken into 8 cm long segments to accomodate a test condition consisting of a 2.5 cm gauge section and two 2.5 cm sections within the grips. This

process limited the number of tests available from each contraction run to a maximum of seven. The fiber segments were then etched as a batch in 98° C fuming nitric acid for ~2 minutes to a final diameter of about 190 μm (7.5 mil). The etch was necessary to remove those surface flaws pre-existing in the as-received fibers and those possibly created by the processing method (cf. Fig. 11). Without the etch, the contracted fibers displayed considerable scatter in tensile strength, ranging from zero to the strength measured after etching. The axial contraction strain produced by etching off a few micrometers of outer sheath layers was estimated to be less than 0.02 percent (5). Thus the etching process in itself had little effect on the stress level for core-initiated fracture.

The tensile strength results for the contracted and etched fibers are shown in Fig. 12. These data are plotted as a function of total contraction strain ϵ_z in order to determine the upper limit for core-compression strengthening. However, because this limit depends strongly on the formation of new sheath flaws which may in turn be more dependent on processing conditions than on the magnitude of ϵ_z, it was decided to distinguish the temperature conditions employed to process the fibers. Therefore, as explained in the legend of Fig. 12, the shape of the data point symbol indicates processing temperature. Because contraction runs were conducted under similar time conditions (30 to 60 min), oxygen conditions can be inferred from the magnitude of ϵ_z; that is, for a given processing temperature, increasing ϵ_z values imply that increasing oxygen volume fractions were employed. Thus data at the lowest contraction for a given temperature were obtained from fibers contracted in impure argon.

The fracture surfaces for all test data of Fig. 12 were examined microscopically in order to establish the fracture source. For the range of

processing conditions studied, three general flaw types were identified by tracing fracture-induced hackle marks back to their sources. As shown by the examples in Fig. 13, these include flaws within the core, flaws near the core-sheath interface, and flaws at the outermost tip of a radial crack within the boron sheath. This last flaw type, commonly referred to as the crack tip flaw, is often observed in boron fibers which are produced at temperatures below 1200° C (8). The source of the radial crack is speculative at the present time, but it may be due to a flaw at the core-sheath interface which initiates lengthwise cleavage in those regions of the sheath which are under residual tensile stresses in the tangential direction (13). The observation of a mirror zone at the tip of the radial crack, as shown in Fig. 13(c), indicated that the radial cracks existed in the contracted fibers before fracture. Thus the radial cracks were created either during the oxidation process, or during cooldown, or during preparations for tensile testing. In fact, a few fibers which were contracted at low temperature split longitudinally during test preparation procedures presumably due to the presence of the radial crack. Fracture surfaces such as that shown in Fig. 13(b) appeared to originate at a flaw located either at the core edge or at the core-sheath interface. The responsible flaw will be referred to as the "near-core" flaw. To distinguish the three flaw types for the Fig. 12 data, open and closed symbols were used for the core flaw and crack tip flaw, respectively, and a slashed open symbol for the near-core flaw.

Although the results of Fig. 12 are limited both in number and variety of processing conditions, they do suggest some general conclusions. For example, whenever a definite core-initiated fracture was observed, the fiber strength was at a level consistent with the model for core compression strengthening. The theoretical range of fiber strengths based on this model

is shown as the area between the two dashed lines. However, for processing temperatures below 900° C, the primary range of this study, core-initiated fractures at contractions above 0.3 percent were not observed due primarily to the formation of the near-core flaw. Thus although the higher oxygen contents in the impure argon allowed faster contractions at temperatures below 900° C, they did not achieve any additional strengthening above 5.5 GN/m^2 (800 ksi). In fact, the upper limit contraction strain for strengthening appeared to decrease as processing temperatures were decreased below 900° C. Using the scant data of Fig. 12, an attempt was made to describe this behavior by the solid curves of Fig. 14. These are approximate plots of the probability of observing core-initiated fractures as a function of processing temperature and total contraction. The dashed curves are extrapolated estimates. With these curves as empirical guidelines, it would appear then that in order to increase the probability for high-strength core fracture at contractions above 0.3 percent, processing temperatures higher than those used in this study should be employed. Whether temperatures above 1000° C, for example, would completely eliminate the near-core and crack-tip flaws remains to be determined, but their use would allow shorter exposure times and thus more cost-effective processing.

Turning to the basic mechanisms for new flaw formation, the Fig. 12 strength data suggest that during processing at a given temperature, the appearance of the near-core flaw preceeded the appearance of the radial crack tip flaw. This sequence supports the model that a flaw at the core-sheath interface is required before the radial crack can propogate under residual tangential stresses within the sheath (13). The existence of the radial crack significantly degrades not only fiber axial strength but also fiber transverse strength as evidenced by the tendency for longitudinal

splitting. It would seem, therefore, that the development of processing conditions which avoided formation of the near-core flaw should also be helpful in eliminating the detrimental radial crack.

Regarding observations on the near-core flaw, the Fig. 12 data suggest that this flaw, like the core flaw, can experience the compressive stresses produced by the oxidation-induced contraction of the sheath. This strength behavior suggests also that according to Griffth fracture theory, the fracture-critical dimension of the near-core flaw, i.e., crack size, changed little with contraction. But in terms of identifying a formation mechanism, perhaps the most important property of the near-core flaw is its location which seems to suggest an origin similar to that of the visible voids of Fig. 9. That is, the near-core flaw may simply be a small void created by rapid boron atom removal away from the core-sheath interface. The fact that Fig. 9 shows no obvious voids around the 17 μm diameter core for contractions below 0.7 percent does not preclude their existence since they may appear randomly and also require a fracture-critical dimension of only 0.1 μm in order to affect boron fiber strength near the 4 GN/m^2 level (6).

If rapid atom diffusion away from the core is indeed the source of the near-core flaw, its formation might be avoided during oxidation processing if atom removal at the fiber surface could be made more rapid than atom diffusion in the sheath. Under this condition, a large concentration gradient of diffusing boron atoms could be established across the sheath radius which should then result in a greater amount of axial contraction before a critical number of boron atoms are removed from the core-sheath interface. The low-temperature high-oxygen approach of this study was probably not successful because, although all diffusion processes were reduced at temperatures below 900° C, surface atom removal through a boron oxide layer was still

slower than atom diffusion in the sheath. As previously discussed, the α data of Fig. 6 suggest that at temperatures above 900° C sheath diffusion may indeed become the limiting process during oxidation processing. Possible reasons for this include an oxide diffusion rate which increases more rapidly with temperature than sheath diffusion and/or a continuous removal of the oxide layer itself due to gravity-induced flow and higher volitility (14). Thus the empirical guidelines of Fig. 14 may just be a reflection of the fact that formation of the near-core flaw during oxidation processing can best be avoided by using thermal conditions which allow boron atom removal at the surface to be more rapid than boron atom removal from the core-sheath interface.

Finally, it is interesting to note that investigators who have employed high temperature processing methods to coat boron fibers with diffusion barriers, such as, boron nitride (15) and boron carbide (16), observed that under certain conditions the coating process increased the average fiber strength by 0.4 to 0.8 GN/m^2 (60 to 120 ksi). The results of the present study suggest that these increases were simply due to flaw compression caused by treatment-induced axial contractions of 0.1 to 0.2 percent. Since the barrier coatings contain boron, contraction was probably produced by atom removal from the sheath as is the case for the formation of boron oxide. Indeed, if one assumes that all the boron for the coating is internally provided by the sheath, Eqs. (5) and (6) can then be used to predict the relationship between barrier coating thickness h_c and axial contraction strain ϵ_z (percent). That is,

$$h_c(\mu m) = \left[\frac{0.0017\ n_c}{\gamma_B \rho_c}\right] \epsilon_z d(\mu m) \qquad (9)$$

where n_c and ρ_c are the atomic weight (gm) and density (gm/cc) of the coating. A significant practical point of this relationship is that by proper choice of coating thickness and fiber diameter, one can control ϵ_z and thus perhaps not only achieve the protective qualities of the barrier but also increase the strength of the base fiber. For example, assuming for all fiber diameters an upper limit for strengthening at $\epsilon_z = 0.3$ percent, Eq. (9) predicts that in order to achieve maximum strength, a B_4C coating on a 142 μm (5.6 mil) fiber should not exceed 0.4 μm. If this thickness should not be sufficient for protective purposes, one could increase the fiber diameter proportionally without paying a strength penalty. Or, as was done by Morin (16), one could increase the coating thickness by externally providing boron atoms by a simultaneous chemical vapor deposition process.

CONCLUDING REMARKS

This investigation concerning the oxidation-induced contraction and strengthening of boron fibers has been useful in several respects. For temperatures between 650° and 900° C, the effects of time, temperature, and oxygen pressure on fiber axial contraction were quantitatively determined so that one can now predict the processing conditions required to produce those contraction strains which result in improved fiber tensile strength. Contraction was only weakly dependent on time (1/2 power) and oxygen content (1/3 power) but, being controlled by a thermally-activated mechanism, was strongly dependent on processing temperature. By combining the high temperature oxidation treatment with a subsequent slight chemical surface etch near 100° C, the average tensile strengths of 203 μm (8 mil) diameter commercial fibers were increased to 5.5 GN/m^2 (800 ksi) with a coefficient-of-variability (COV) of less than 5 percent. This strength level was

achieved by a compression of strength-limiting flaws within the fiber's tungsten boride core at an axial contraction strain of 0.3 percent. Since the average tensile strength and COV of the as-received fibers were about 3.4 GN/m^2 (500 ksi) and 15 percent, respectively, the combined use of these processing methods more than doubled not only the minimum fiber tensile strength but also the average tensile work of fracture. At the present time, a strengthening limit exists at 0.3 percent contraction due to the formation of flaws near the core-sheath interface. The trend of the fracture data suggest, however, that the use of oxidation processing temperatures above 900° C may delay this flaw formation effect until higher contraction and strength levels.

The physical mechanism responsible for boron fiber contraction appears to be the removal of boron atoms from inner surfaces within the CVD boron sheath, such as, the boundary surfaces between kernels. These inner surface atoms rapidly diffuse to the external fiber surface to replace other boron atoms lost by reaction with oxygen. In so doing, atoms are removed from around the tungsten-boride core, thus probably creating the detrimental flaws responsible for the strength dropoff at contractions above 0.3 percent. At temperatures between 650° and 900° C, the boron atom removal rate from the fiber is not limited by inner sheath diffusion but by atomic diffusion through a thin boron oxide layer on the fiber surface. The contraction kinetics reflect the growth of this layer and thus can be used to obtain information concerning boron fiber oxidation in this temperature range. Finally, because the processes involved in oxide growth are similar to those that occur during formation of boron-containing diffusion barrier coatings such as boron carbide, it should now be possible in light of the

above results not only to understand the effects of the coating process on sheath microstructure but also to predict optimum processing conditions for achieving coated fibers with average strength levels near 5.5 GN/m^2 (800 ksi).

REFERENCES

1. L. E. Dardi and K. G. Kreider, pp. 231-270 in Failure Modes in Composites, edited by I. Toth, The Metallurgical Society of AIME, New York, 1973.
2. C. C. Chamis, M. P. Hanson, and T. T. Serafini, pp. 324-349 in Composite Materials: Testing and Design (Second Conference), ASTM STP 497, American Society for Testing and Materials, Philadelphia, 1972.
3. F. E. Wawner, Jr., pp. 283-300 in Boron: Preparation, Properties, and Applications, edited by G. K. Gaule, Plenum Press, New York, 1965.
4. R. J. Smith, "Changes in Boron Fiber Strength due to Surface Removal by Chemical Etching," NASA TN D-8219, 1976.
5. J. A. DiCarlo, "Techniques for Increasing Boron Fiber Fracture Strain," NASA TM X-73627, 1977.
6. J. A. DiCarlo, "Mechanisms of Boron Fiber Strengthening by Thermal Treatment," NASA TM-79077, 1979.
7. F. E. Wawner, Jr., J. W. Eason, and R. A. Johnson, "Investigation of Elongation and its Relationship to Residual Stresses in Boron Filaments," University of Virginia, Charlottesville, Report No. UVA/525322/MS79/102, 1979. AD-A074440.
8. V. Krukonis, pp. 517-540 in Boron and Refractory Borides, edited by V. I. Matkovich, Springer-Verlag, Berlin, 1977.
9. J. A. DiCarlo, pp. 443-465 in Composite Materials: Testing and Design, ASTM STP 617, American Society for Testing and Materials, Philadelphia, 1977.

10. J. A. DiCarlo, pp. 520-538 in ICCM/2, Second International Conference on Composite Materials, edited by B. R. Noton, The Metallurgical Society of AIME, Warrendale, PA, 1978.

11. K. Hauffe, Oxidation of Metals, Plenum Press, New York, 1965.

12. N. P. Nies and G. W. Campbell, pp. 53-231 in Boron, Metallo-Boron Compounds and Boranes, edited by R. Adams, Interscience, New York, 1964.

13. J. Vega-Boggio and O. Vingsbo, "Radial Cracks in Boron Fibers," J. Mater. Sci., 12, 2519-2524, 1977.

14. C. P. Talley, "Combustion of Elemental Boron," Aero Space Eng., 18, 37-41, 1959.

15. J. L. Camahort, V. J. Krukonis, and F. W. Wawner, "Low Cost B-Al Composites by Cast Tape," SAMPE Q., 6, 40-43, 1975.

16. D. Morin, "Boron Carbide-Coated Boron Filament as Reinforcement in Aluminum Alloy Matrices," J. Less-Common Met., 47, 207-213, 1976.

TABLE I. - GAS ANALYSIS IN

VOLUME PERCENT

	Argon	Oxygen
Argon	balance	0.04
Oxygen	0.01	balance
Nitrogen	.05	0.40
Hydrogen	.10	.05
Carbon dioxide	0	.10

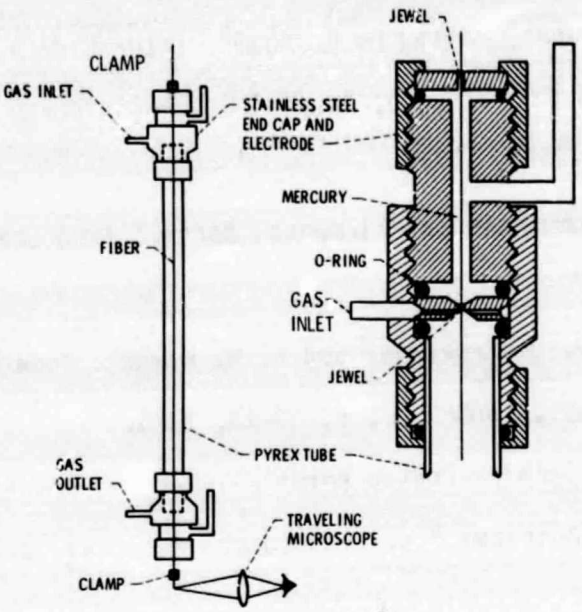

Figure 1. - Schematic of apparatus employed to heat treat boron fibers in a gas environment and simultaneously measure changes in fiber length.

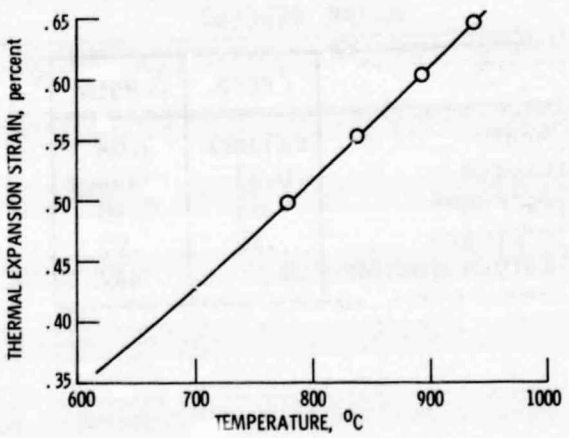

Figure 2. - Thermal expansion strain of 203 μm diameter boron fibers.

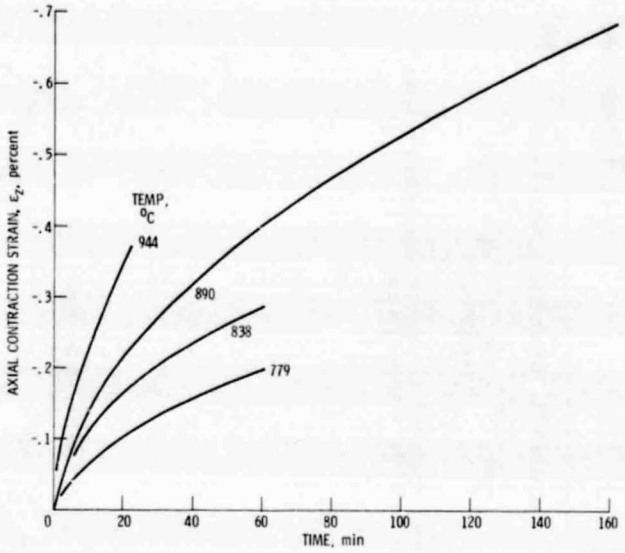

Figure 3. - Typical axial contraction strain data measured during heat treatment of 203 μm boron fibers in impure argon gas.

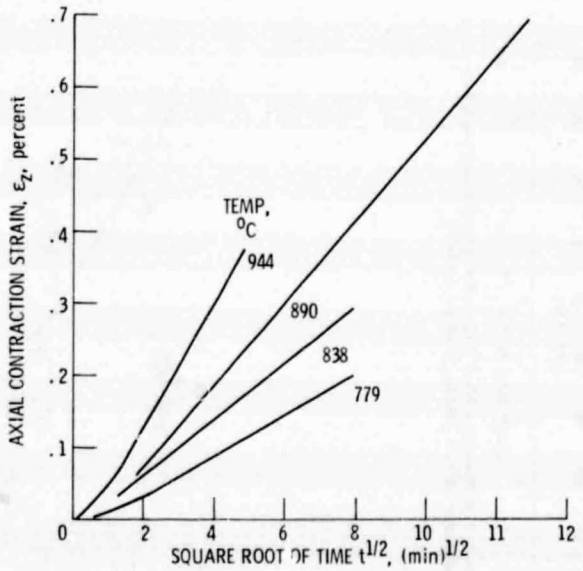

Figure 4. - The parabolic time dependence of axial contraction strair, observed during heat treatment of 203 μm boron fibers in impure argon gas.

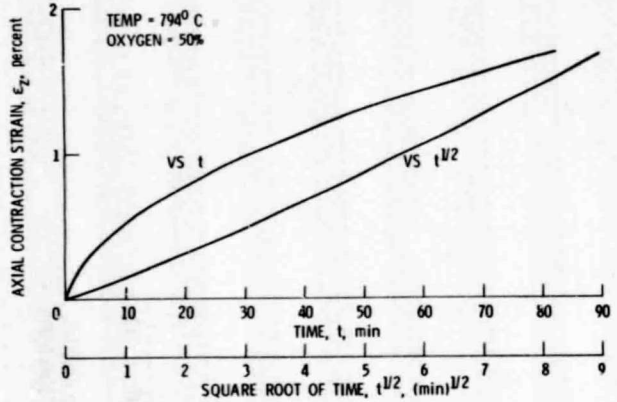

Figure 5. - The axial contraction of 203 μm boron fibers measured during heat treatment at 794° C in a 50% oxygen-argon gas mixture.

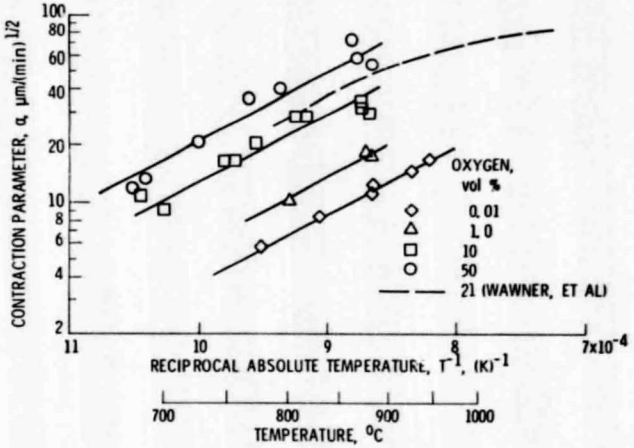

Figure 6. - Temperature and oxygen dependence for the α parameter governing boron fiber axial contraction.

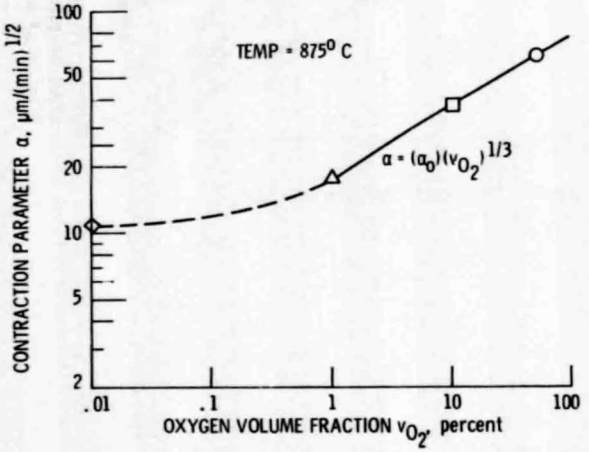

Figure 7. - Oxygen dependence for the α parameter governing boron fiber axial contraction.

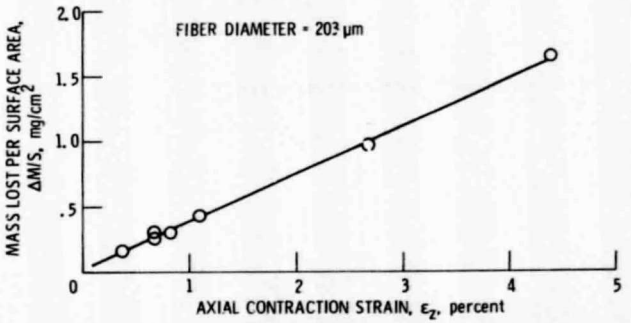

Figure 8. - The mass lost per unit surface area during oxidation-induced axial contraction of 203 μm boron fibers.

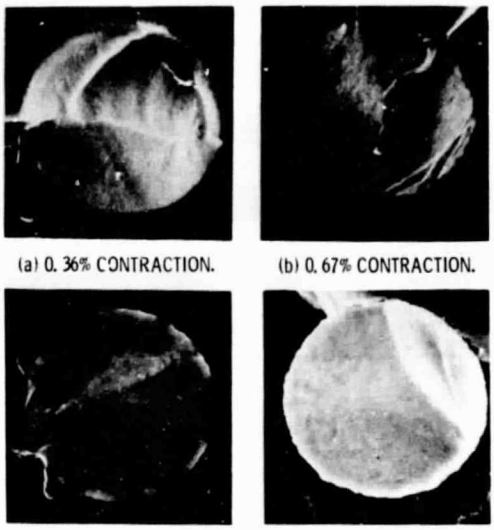

(a) 0.36% CONTRACTION. (b) 0.67% CONTRACTION.

(c) 1.09% CONTRACTION. (d) 4.4% CONTRACTION.

Figure 9. - SEM photographs of the effects of oxidation-induced axial contraction on void growth around the 17 μm diameter core of 203 μm diameter boron fibers.

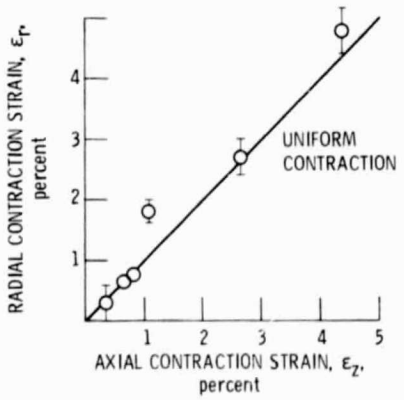

Figure 10. - The radial contraction strain measured for 203 μm boron fibers after oxidation-induced axial contraction and removal of surface boron oxide layers.

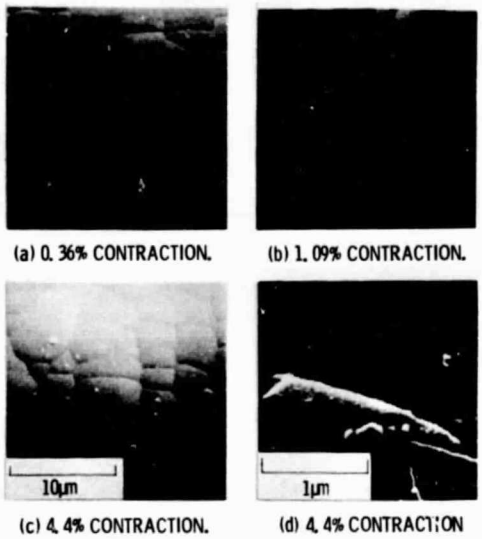

(a) 0.36% CONTRACTION. (b) 1.09% CONTRACTION.

(c) 4.4% CONTRACTION. (d) 4.4% CONTRACTION

Figure 11. - SEM photographs of the surfaces of 203 μm diameter boron fibers after heat treatment in oxygen and subsequent cleaning in methanol to remove boron oxide layers.

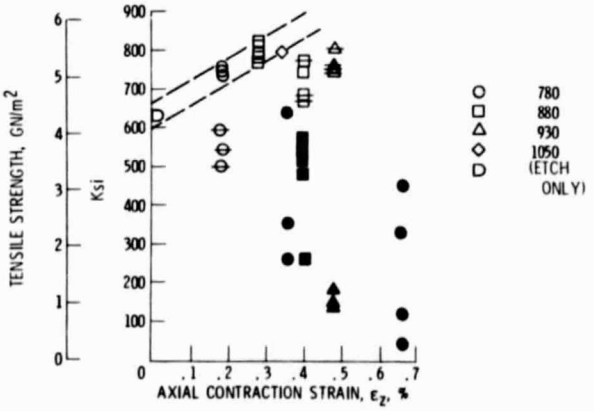

Figure 12. - Effects of oxidation-induced contraction on the tensile strength of 203 μm boron fibers after a slight etch to a final diameter of ~ 190 μm. Fracture initiation sites: core - open symbols, near-core - slashed symbols, radial crack tip - closed symbols.

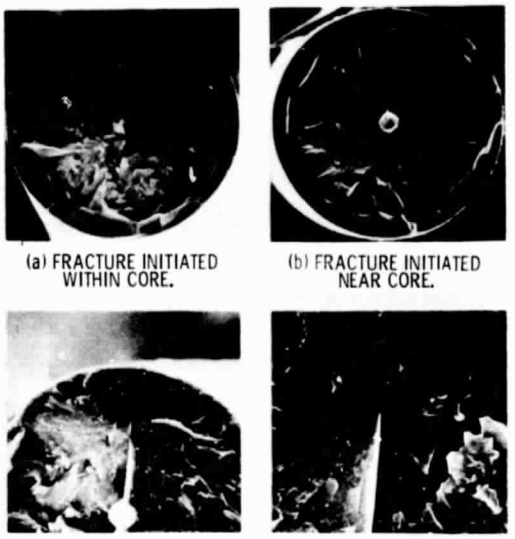

Figure 13. - SEM photographs of the fracture surfaces of 203 μm diameter boron fibers after heat treatment in oxygen and subsequent slight etching to a final diameter of ~ 190 μm.

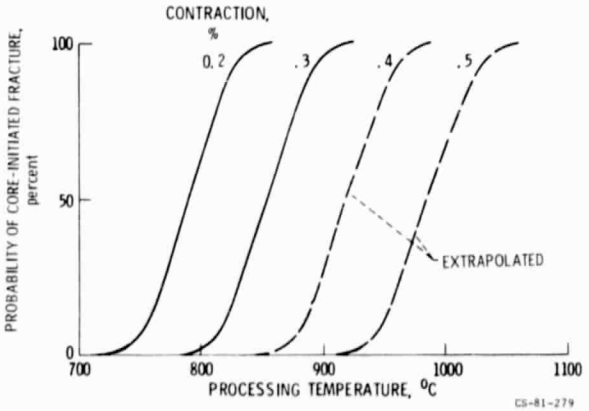

Figure 14. - Approximate (solid) and extrapolated (dashed) curves for the effects of processing temperature and oxidation-induced contraction strain on the probability of observing high strength core-initiated fracture in slightly etched 203 μm boron fibers.